

# A model of the upper branch of the meridional overturning of the southern ocean

John Marshall \*, Timour Radko

*Department of Earth, Atmospheric and Planetary Sciences, Massachusetts Institute of Technology, 77 Massachusetts Avenue, Cambridge, MA 02139, United States*

Received 21 September 2004; received in revised form 8 May 2005; accepted 25 April 2006  
Available online 28 August 2006

---

## Abstract

A zonal-average model of the upper branch of the meridional overturning circulation of the southern ocean is constructed and used to discuss the processes – wind, buoyancy, eddy forcing and boundary conditions – that control its strength and sense of circulation. The geometry of the thermocline ‘wedge’, set by the mapping between the vertical spacing of buoyancy surfaces (the stratification) on the equatorial flank of the Antarctic Circumpolar Current and their outcrop at the sea surface, is seen to play a central role by setting the interior large-scale potential vorticity distribution. It is shown that the action of eddies mixing this potential vorticity field induces a residual flow in the meridional plane much as is observed, with upwelling of fluid around Antarctica, northward surface flow and subduction to form intermediate water. Along with this overturning circulation there is a concomitant air-sea buoyancy flux directed in to the ocean.

© 2006 Elsevier Ltd. All rights reserved.

*Keywords:* Meridional overturning circulation; Antarctic circumpolar current; Southern ocean

---

## 1. Introduction

Fig. 1 presents a schematic diagram of a zonal-average view of the upper and lower branches of the global meridional overturning circulation (MOC) of the southern ocean. Southward flowing circumpolar deep water is partitioned in to upper and lower branches. Upper circumpolar deep water is imagined to upwell to the surface and return northward in a surface boundary layer. Lower circumpolar deep water circulates in a lower branch exposed to convective/diabatic processes occurring around Antarctica and mixing in the bottom boundary layer. The figure is highly schematized and many of the details are uncertain. Nevertheless it represents a consensus view that was first synthesized by Sverdrup et al. (1942) and reviewed by Speer et al. (2000) and Rintoul et al. (2001).

Recently a theoretical framework has been developed to describe the zonal flow of the southern ocean and its attendant overturning circulation. As described in Marshall and Radko (2003) – see also Olbers and Visbeck

---

\* Corresponding author. Tel.: +1 617 253 9615; fax: +1 617 253 4464.  
E-mail address: [jmarsh@mit.edu](mailto:jmarsh@mit.edu) (J. Marshall).

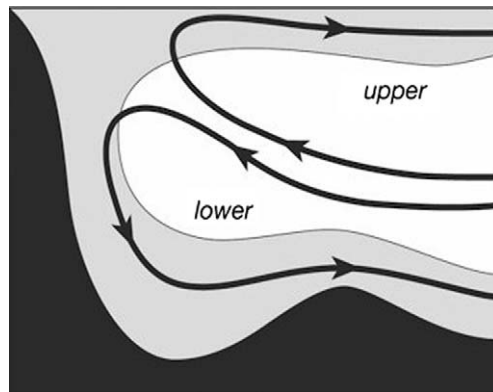


Fig. 1. A schematic diagram of the overturning circulation in the southern ocean. Southward flowing circumpolar deep water is partitioned into upper and lower branches. Upper circumpolar deep water is imagined to upwell to the surface and return northward in a surface boundary layer. Lower circumpolar deep water circulates in a lower branch exposed to convection/mixing processes occurring around Antarctica and in the bottom boundary layer. Mixing and diabatic processes are imagined to be confined to the regions shaded light grey.

(2005) – the absence of zonal boundaries in the southern ocean has enabled the meteorologist’s zonal-average residual-mean theory to be applied to develop conceptual models that draw together in suggestive ways, the relative roles of wind, buoyancy and eddy forcing in setting the stratification, transport and overturning circulation of the southern ocean.

Our model of circumpolar flow and its overturning circulation is offered in the same spirit as that of Luyten et al.’s (1983) – hereafter LPS – description of the thermocline ventilation ocean gyres. As in LPS, surface conditions are propagated down in to the interior under assumed dynamics. The dynamical balances are very different, however. Unlike LPS we cannot build a construction around Sverdrup balance because of the absence of meridional boundaries in the southern ocean. Instead we are dealing with a thermocline whose stratification is fundamentally controlled by eddy dynamics, as in the models of Marshall et al. (2002), Marshall and Radko (2003) or Cessi and Fantini (2004). The theoretical framework is provided by residual-mean theory. Rather than adopt the refinements due to McDougall and McIntosh (1996, 2001) in this zonal-average application we use the ‘standard’ framework reviewed (Andrews and McIntyre, 1976) in (Andrews et al. (1987)). There the residual momentum equation takes on a particularly simple and attractive form and clearly draws out and connects the role of eddy potential vorticity fluxes in driving meridional overturning circulation.

In this paper we make use of the residual-mean theory of the ACC and its overturning circulation developed in Marshall and Radko (2003) (hereafter MR) and apply it to study the processes at work in setting the structure of the upper branch in Fig. 1. We extend MR’s model to handle more general boundary conditions which, in particular, allow us to specify conditions on the equatorward flank of the southern ocean where – see Fig. 1 – fluid is exchanged with the rest of the world ocean. The air-sea buoyancy flux need no longer be prescribed, as was done in MR’s diagnostic model, but becomes part of the solution. We are particularly interested in the connection between the ‘pull’ associated with Ekman drift imparted by surface westerlies discussed in Toggweiler and Samuels (1998) and the ‘push’ due to interior inflow of upper circumpolar deep water. This role of the southern ocean and eddies therein, is the goal of the conceptual model of Gnanadesikan (1999): dynamics interior to the ACC can have global repercussions but the ACC is also part of the global circulation and hence influenced by it. We return to these global connections in the conclusions.

The paper is set out as follows. In Section 2 we review background observations and theory. The theoretical framework is set out in much more detail in MR: here, however, we briefly introduce the underlying ideas so as to present a more-or-less self contained discussion. In Section 3 we apply residual-mean theory to develop ideas about what controls the sense of circulation and strength of the upper cell. In Section 4 we present some detailed solutions which considerably extend those found in MR and, in particular, address aspects of the (two-way) connection between the ACC and the rest of the ocean. In Section 5 we conclude.

## 2. Background

### 2.1. Observations

The surface geostrophic streamfunction computed from altimetry and the large-scale buoyancy structure of the southern ocean is shown in Fig. 2. Buoyancy surfaces are seen to extend up to the surface, outcropping around Antarctica. The along-stream current is in thermal wind balance with this interior cross-stream buoyancy gradient. The streamwise average wind-stress driving the ACC is shown in Fig. 3(top). The stress increases moving equatorwards across the stream to reach a maximum just equatorward of the region of circumpolar flow delineated by the thick lines snaking around Antarctica in Fig. 2(top). The buoyancy distribution at the

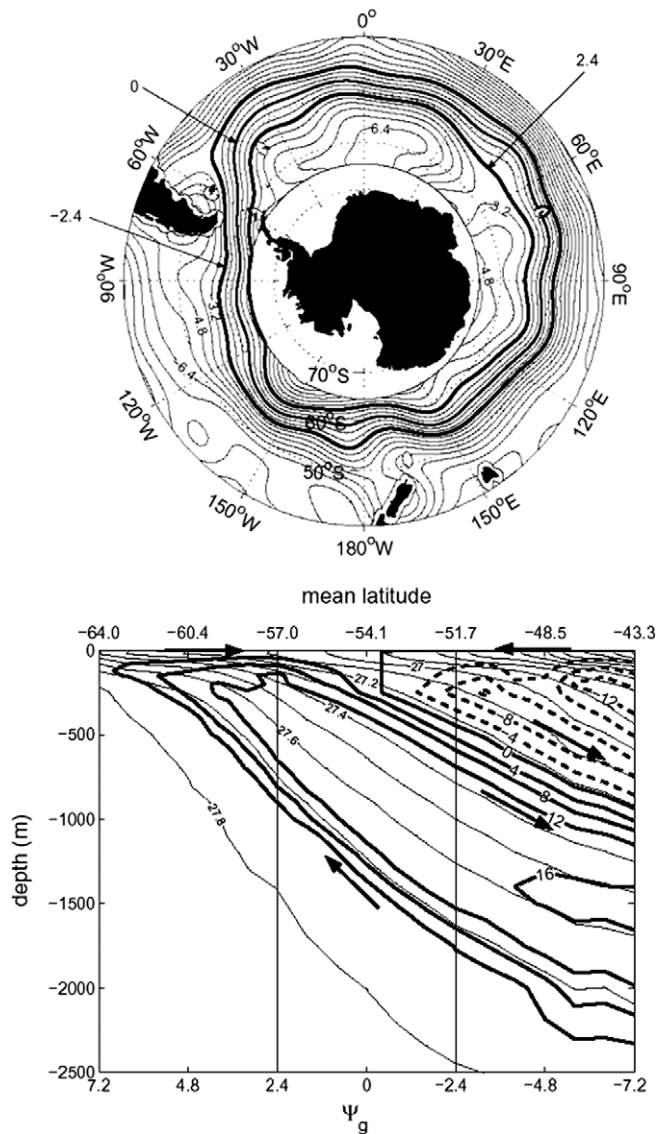


Fig. 2. (Top) Climatological surface geostrophic streamfunction as observed by altimetry. (Bottom) Estimate of the upper branch of the residual overturning circulation in the southern ocean due to Karsten and Marshall (2002a). The residual streamfunction is plotted in Sverdrups. The contour interval is 4 Sv with solid (dashed) contours indicating positive (negative) values. The arrows mark the direction of flow. The faint lines are contours of neutral density with a contour interval of 0.2.

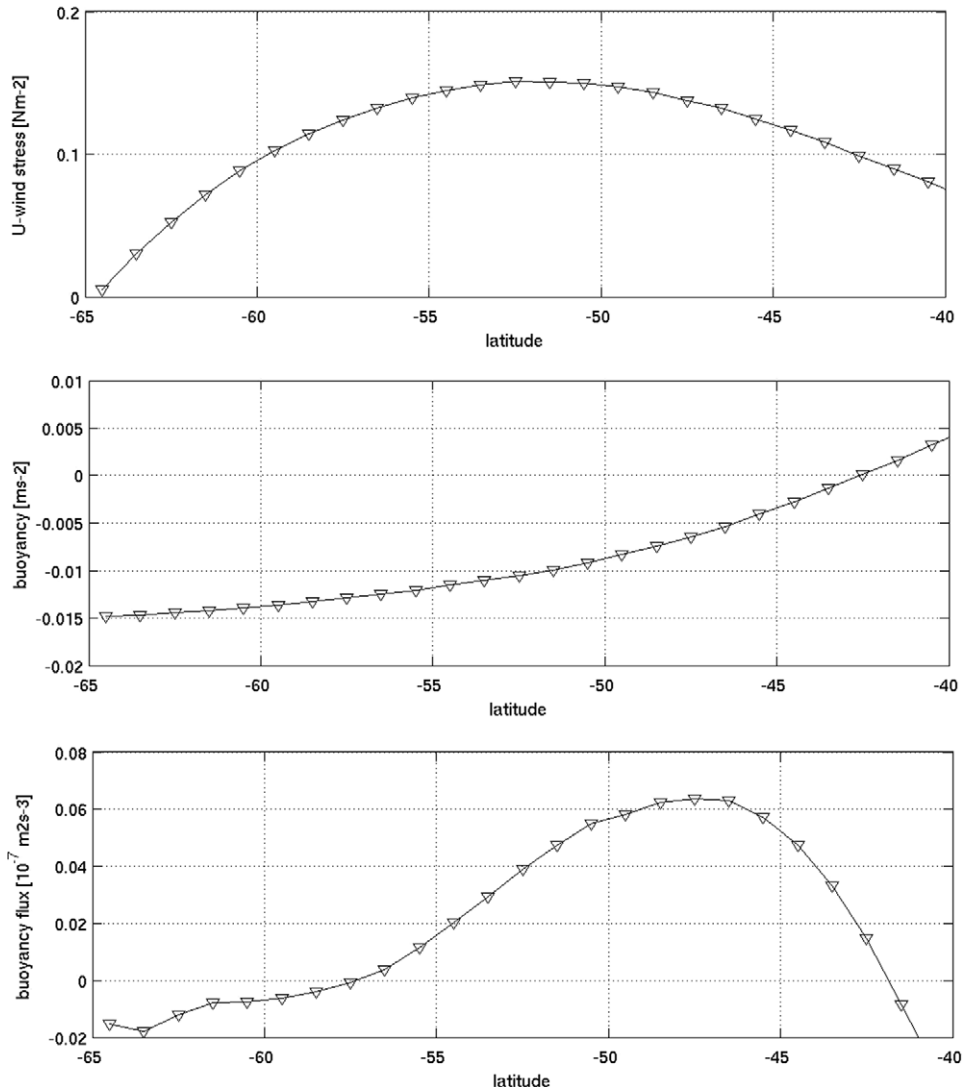


Fig. 3. Observed (top) wind stress (middle) surface buoyancy and (bottom) air-sea buoyancy flux (positive is in to the ocean) over the southern ocean. All observations are streamwise-averaged along the time-mean streamlines shown in Fig. 2(top). The region of circumpolar flow is between 51.7° S and 57° S, as indicated in Fig. 2(bottom).

surface (again averaged along geostrophic streamlines) is shown in Fig. 3(middle) and reveals a more-or-less linear increase in buoyancy moving equatorwards across the stream from Antarctica. The air-sea buoyancy flux is plotted in the bottom panel: generally there is a flux into the ocean, providing the buoyancy required to allow water parcels upwelling around Antarctica to eventually subduct in a much lighter density range, that of Antarctic Intermediate Water.

The pattern of meridional overturning circulation,  $\Psi_{\text{res}}$ , in the southern ocean is much less certain. A number of attempts have been made to infer it from observations – see the review of Rintoul et al. (2001) – using box inverse methods (e.g. Sloyan and Rintoul, 2001), from air-sea fluxes (using Eq. (5) of Section 2.2 as in Speer et al., 2000) and from observation of surface winds and satellite altimetry, making use of residual-mean theory Karsten and Marshall (2002a). Fig. 2(bottom), from Karsten and Marshall (2002a), shows their estimate of the upper branch of the MOC in the southern ocean. They find upwelling of upper circumpolar deep water around Antarctica of some 16 Sv, equatorward flow at the surface (associated with input of buoyancy from the atmosphere) and subduction of perhaps 20 Sv of Antarctic Intermediate Water just equatorward of

the ACC. This is the upper branch of the southern ocean limb of the MOC. The goal of the present paper is to understand the relationship between the outcrops at the surface, the pattern of wind and buoyancy fluxes over the southern ocean, the interior stratification and the associated pattern of meridional overturning.

*2.2. Theoretical framework*

We frame our discussion in terms of a two-dimensional (streamwise-averaged) model of the southern ocean in which the buoyancy distribution, air-sea fluxes and wind-stress forcing over the circumpolar ocean are integrated along time-mean streamlines (as in Fig. 3) and so only vary in the cross-stream direction.

Following MR, we adopt a transformed Eulerian-mean formulation (Andrews et al., 1987), in which tracer and momentum budgets are written in terms of a residual overturning streamfunction and associated velocities

$$\psi_{\text{res}} = \bar{\psi} + \psi^* \tag{1}$$

$$(v_{\text{res}}, w_{\text{res}}) = \left( -\frac{\partial \psi_{\text{res}}}{\partial z}, \frac{\partial \psi_{\text{res}}}{\partial y} \right) \tag{2}$$

where  $(v_{\text{res}}, w_{\text{res}})$  is the residual meridional and vertical flow expressed in terms of the residual streamfunction made up of  $\bar{\psi}$ , the time-mean overturning streamfunction and  $\psi^*$ , the streamfunction associated with eddies. Our focus on the residual flow makes sense because in a highly eddying region of the ocean such as the ACC, it is the residual flow rather than the Eulerian-mean flow that advects tracers.

The residual-mean buoyancy equation can be written

$$J_{y,z}(\psi_{\text{res}}, \bar{b}) = \frac{\partial \tilde{B}}{\partial z} \tag{3}$$

where  $J_{y,z}(\psi_{\text{res}}, \bar{b}) = (\psi_{\text{res}})_y \bar{b}_z - (\psi_{\text{res}})_z \bar{b}_y = \mathbf{v}_{\text{res}} \cdot \nabla \bar{b}$ , the residual streamfunction  $\psi_{\text{res}}$  is given by Eq. (1) and  $\tilde{B}$  is the buoyancy forcing due to air-sea fluxes, small-scale mixing and diabatic eddy fluxes – see the discussion in MR. To progress further we make some simplifying assumptions. We suppose that in the main thermocline buoyancy forcing vanishes (due both to convection and mixing processes) –  $\tilde{B} = 0$  in (3). Thus

$$J(\psi_{\text{res}}, \bar{b}) = 0 \text{ interior} \tag{4}$$

implying that there is a functional relationship between  $\psi_{\text{res}}$  and  $\bar{b}$ :  $\psi_{\text{res}} = \psi_{\text{res}}(\bar{b})$ . This functional relationship will be set, we suppose, in the surface mixed layer where  $\psi_{\text{res}}$  crosses isopycnals – see Fig. 4. Furthermore we assume that the mixed layer is vertically homogeneous and of constant depth,  $h_m$ , (as sketched in Fig. 4), set entrainment fluxes at its base to zero ( $\tilde{B}_{-h_m} = 0$ ) and neglect the seasonal cycle. Then, integrating Eq. (3) over the depth of the mixed layer ( $h_m$ ), we obtain (see Marshall, 1997)

$$\psi_{\text{res}}|_{z=-h_m} \frac{\partial b_m}{\partial y} = \tilde{B}_0, \tag{5}$$

where  $b_m$  is the surface buoyancy, and  $\tilde{B}_0$  is the net buoyancy supplied to the mixed layer by air-sea buoyancy fluxes and the lateral (diabatic) eddy fluxes in the mixed layer. Eq. (5) makes it clear that information about  $\psi_{\text{res}}$  can be obtained by inspection of the surface buoyancy distribution and surface buoyancy fluxes, as exploited by Speer et al. (2000).

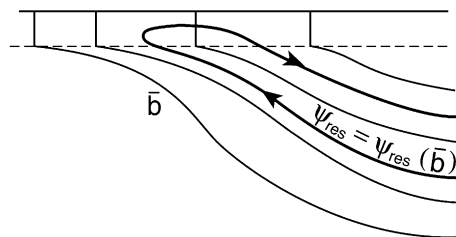


Fig. 4. The residual flow  $\psi_{\text{res}} = \bar{\psi} + \psi^*$  is assumed to be directed along mean buoyancy surfaces,  $\bar{b}$ , in the interior, but have a diapycnal component in the mixed layer of depth  $h_m$  (denoted by the horizontal dotted line).

The Eulerian-mean streamfunction is given by Ekman theory thus

$$\bar{\psi} = -\frac{\tau_0}{f} \quad (6)$$

where  $\tau_0$  is the surface wind stress and  $f$  is the Coriolis parameter, both varying in the cross-stream direction,  $y$ .

Finally, in the stratified interior, residual-mean theory relates the eddy-streamfunction to eddy buoyancy fluxes thus

$$\psi^* = \frac{\overline{v'b'}}{\overline{b_z}}. \quad (7)$$

Noting that  $h' \sim \frac{h'}{b_z}$  (where  $h$  is the displacement of  $b$  surface),  $\psi^*$  has obvious connections to the ‘bolus’ transport  $\overline{v'h'}$ .

This, then, is a brief description of the dynamical framework that will be used to discuss the southern ocean overturning circulation. We will now use it to derive some simple illustrative solutions.

### 3. Models of the overturning circulation

To develop a diagnostic model of the overturning circulation, one must express  $\psi^*$  in Eqs. (1) and (7) in terms of  $\bar{b}$ . In other words it is necessary to specify how the eddy fluxes depend on the time-mean quantities. Following Visbeck et al. (1997), we suppose that  $\psi^*$  depends on the isopycnal slope thus<sup>1</sup>

$$\psi^* = \frac{\overline{v'b'}}{\overline{b_z}} = k_0 |s_\rho| s_\rho \quad (8)$$

where we have supposed that interior eddy fluxes are adiabatic,  $s_\rho = -\frac{\bar{b}_y}{\bar{b}_z}$  is the slope of the isopycnals and  $k_0$  is a scaling constant which depends on the efficiency of eddies (see MR). Combining Eqs. (8), (1) and (6), we find that the residual streamfunction can now be expressed thus

$$\psi_{\text{res}}(b) = -\frac{\tau_0}{f} + k_0 |s_\rho| s_\rho \quad (9)$$

or, making  $s_\rho$  the subject of the equation

$$s_\rho = -\sqrt{\left(-\frac{\tau_0}{fk_0} - \frac{\psi_{\text{res}}(b)}{k_0}\right)} \quad (10)$$

This simple relation tells us that if we know  $\psi_{\text{res}}$  (from, say, Eq. (5)) and  $\tau_0(y)$ , we can construct the interior stratification  $b(y, z)$  because  $\psi_{\text{res}} = \psi_{\text{res}}(b)$  at the surface.

Eqs. (5) and (10) are the key relationship of MRs model. We now go on to discuss how we can use them to relate together the wind field, the air-sea buoyancy flux, the residual flow and the stratification (and hence the thermal wind zonal current) of the southern ocean. Before presenting explicit solutions we consider some instructive reference cases.

#### 3.1. The limit of vanishing residual overturning

It is very instructive to consider the limit of vanishing MOC:  $\psi_{\text{res}} \rightarrow 0$  in Eq. (9), so that  $\tau_0 = f\psi^*$  – eddy form drag balances wind stress, as first discussed by Johnson and Bryden (1989). In this case  $s_\rho = \frac{dz}{dy} = -\sqrt{-\frac{\tau_0}{fk_0}}$  in Eq. (10) and the isopycnal slope only depends on  $\frac{\tau_0}{f}$ .

Suppose for a moment that  $\tau_0$  and  $f$  are constant, so that  $\frac{\tau_0}{f}$  is constant everywhere, and hence  $s_\rho$  is everywhere constant. Then, as shown in Fig. 5, the isopycnals are straight lines with a constant slope. If  $\frac{\tau_0}{f}$  varies in  $y$

<sup>1</sup> The important point here is that we assume  $\Psi^* = \Psi^*(s_\rho)$  and choose a function that ensures that  $\Psi^*$  is in the sense to flatten isopycnals. The precise form chosen in Eq. (8) is motivated by the arguments given in Visbeck et al. (1997) and by recent laboratory experiments reported in Cenedese et al. (2004).

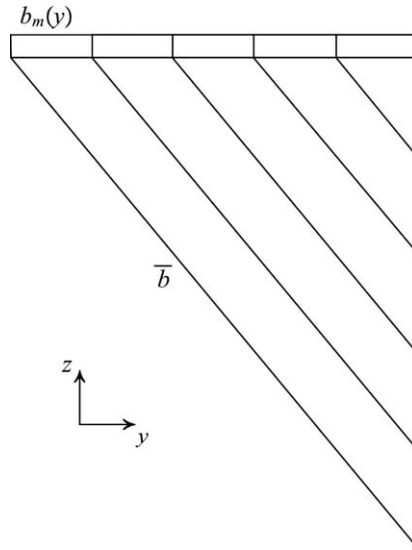


Fig. 5. Depth of isopycnals for a uniform PV solution on the ‘ $f$ ’ plane in which the surface wind stress is assumed constant.  $\psi_{\text{res}}$  is zero, as is the air-sea buoyancy flux, in contrast to Fig. 7.

the isopycnal slope varies in  $y$  but not in  $z$ : thus the isopycnal surfaces remain parallel to one another but they are no longer straight lines

$$z = s_{\rho-b_m}(y)y \tag{11}$$

where  $s_{\rho-b_m}(y) = -\sqrt{\frac{1}{k_0} \left| \frac{\tau_0}{f} \right|}$  is the slope of the isopycnals at the base of the mixed layer set by the balance between the wind-stress overturning isopycnals and eddies trying to flatten them out (as realized in the laboratory experiments of Marshall et al. (2002) and Cenedese et al. (2004)). Such solutions are shown in Figs. 5 and 6 of MR. However, it is clear that these  $f$ -plane constant PV solutions<sup>2</sup> will always fail to capture a notable aspect of the observed meridional structure of the thermocline: they map down an essentially linear meridional buoyancy distribution at the surface (see Fig. 3 middle) to another linear vertical buoyancy distribution on the equatorial flank of the ACC. Observations of the stratification of the southern ocean, however, show that  $N^2$  is not uniform with depth but much, much stronger near the surface. For example, Karsten and Marshall (2002b), in an observational study of the equivalent barotropic structure of the ACC, show that the observed vertical buoyancy distribution in the southern ocean is well represented by exponentials that decay with depth. One such buoyancy profile, on the equatorward flank of the ACC, is shown in Fig. 6, together with its ‘best fit’ exponential profile. The exponential fit is excellent. The lower panel of Fig. 6 shows that the e-folding decay scale of the buoyancy field increases on moving equatorwards across the stream, reflecting the deepening of the thermocline as evident in Fig. 2(bottom).

### 3.2. Non-zero residual overturning solutions

The constant PV solutions just described map the prescribed surface buoyancy field,  $b_m(y)$ , down in to the interior following Eq. (11). They all have  $\Psi_{\text{res}} = 0$  and  $B_0 = 0$ . But what happens if the observed vertical stratification on the equatorial flank,  $b_N(z)$ , does not ‘fit’ with that mapped down from the surface? For  $b_m(y)$  to map down on to a more general form of  $b_N(z)$ , the interior PV distribution cannot be constant on  $b$  surfaces and, as we shall see,  $\psi_{\text{res}}$  will no longer be zero. This non-zero  $\psi_{\text{res}}$  will also imply a non-zero air-sea buoyancy flux. Moreover we will be able to adjust  $\psi_{\text{res}}$  to bring the  $b_m(y)$  and  $b_N(z)$  in to consistency with one another.

<sup>2</sup> Constant PV solutions of the  $\beta$ -plane are discussed in the Appendix.

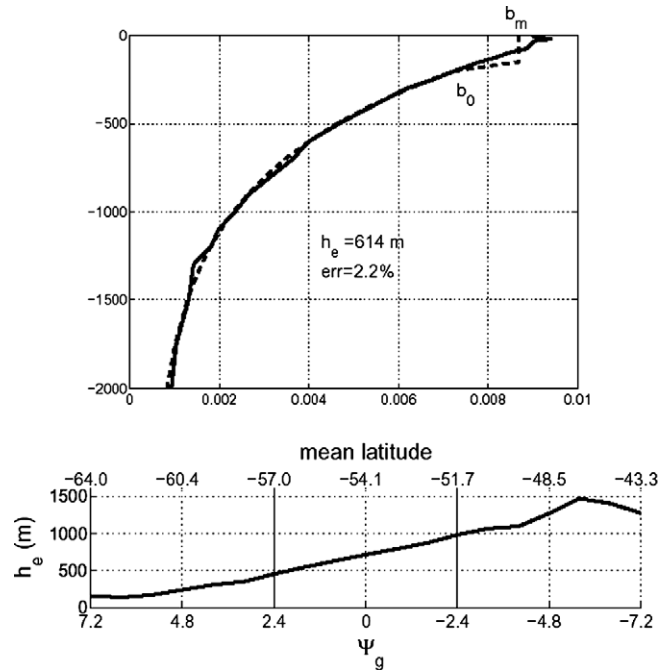


Fig. 6. A decaying exponential fitted to the observed vertical buoyancy distribution on the equatorward flank of the ACC.

It is instructive to again consider the case of constant  $\frac{\sigma}{f}$ . If  $\psi_{\text{res}}$  is constant along  $b$  surfaces in the interior, as assumed here, then the  $b$  surfaces are again straight lines! In the schematic diagram, Fig. 7, ‘straight lines’ are used to join a linear surface distribution on to a vertical profile on the equatorial flank in which the stratification is surface intensified. The deeper of the shaded layers, perforce, thins on moving toward the pole: the

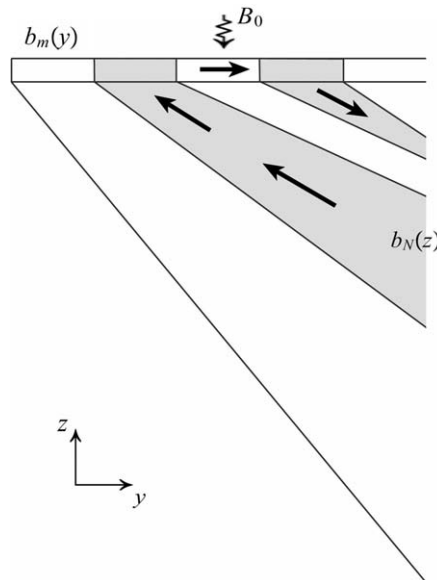


Fig. 7. A linear surface buoyancy distribution is mapped on to an exponential vertical distribution on the equatorial flank of the domain using straight lines, appropriate if  $\frac{\sigma}{f}$  is constant in Eq. (10). The sign of the meridional isentropic potential vorticity gradient thus changes sign, as revealed by the shaded regions. The straight arrows indicate the sense of the residual circulation; the wiggly arrow the sense of the air-sea buoyancy flux.

upper shaded layer thickens on moving toward the pole. In other words there are interior potential vorticity gradients directed in opposite direction. Moreover, eddies acting on these interior PV gradients must drive non-zero residual flow. In the particular context of the eddy closure used here, differentiating Eq. (9) with respect to  $z$  and using Eq. (2), the meridional residual flow is

$$v_{\text{res}} = -2k_0|s_\rho| \frac{\partial s_\rho}{\partial z} \tag{12}$$

Inspecting Fig. 7 we see that in the lower part of the column  $\frac{\partial s_\rho}{\partial z} > 0$  (remembering that  $s_\rho < 0$ ) and hence  $v_{\text{res}} < 0$ ; in the upper part of the column  $\frac{\partial s_\rho}{\partial z} < 0$  and hence  $v_{\text{res}} > 0$ . We thus must obtain a residual circulation as indicated by the arrows in Fig. 7 – i.e. in the sense suggested by observations.

If one believes that eddies flux PV down the large-scale gradient (Rhines and Young, 1982),  $\psi_{\text{res}}$  is an inevitable and rather general consequence of eddies acting on the geometry of the isopycnal surfaces – the residual momentum equation in isentropic coordinates is (in the absence of applied stresses, appropriate to the interior of the water column)

$$-fv_{\text{res}} = \overline{v'Q'}$$

where  $v_{\text{res}}$  is the residual flow on an isentropic surface and  $\overline{v'Q'}$  is the meridional isentropic eddy PV flux. Thus if  $\overline{v'Q'} = -K \times \text{IPV}$ , where IPV is the isentropic potential vorticity gradient and  $K$  is an eddy transfer coefficient, then  $v_{\text{res}} = \frac{K \times \text{IPV}}{f}$  – i.e. isentropic PV gradients imply meridional residual flow, as sketched in Fig. 7.

We thus see that the sense of the residual flow is controlled by interior PV gradients and hence the mapping between  $b_m(y) \leftrightarrow b_N(z)$ . Moreover, because  $\psi_{\text{res}} \neq 0$  in the presence of IPV gradients, by Eq. (5), there must be an implied air-sea buoyancy flux which we can also diagnose and compare with observations.

#### 4. Explicit solutions

We now present explicit solutions in which the mapping  $b_m(y) \leftrightarrow b_N(z)$  is used to infer  $\psi_{\text{res}}$  and the air-sea buoyancy flux, given a surface wind pattern,  $\tau_0(y)$ . In the first solution we prescribe the surface buoyancy distribution. In the second we compute it as part of the solution.

##### 4.1. Prescribing the surface buoyancy distribution

Based on an analysis of observations, such as those shown in Fig. 3, which involves interpolating fields on to a coordinate system aligned with the ACC, we set

$$\begin{cases} b_m(y) = (y/L_y)\Delta b, & \Delta b = 0.015 \text{ m s}^{-2} \\ \tau_0(y) = \tau_{00} \left[ 0.6 + \sin\left(\pi \frac{y}{L_y}\right) \right], & \tau_{00} = 0.00015 \text{ m}^2 \text{ s}^{-2} \end{cases} \tag{13}$$

These are slightly modified relative to those used in MR to better match the observations. The Coriolis parameter is  $f(y) = f_0 + \beta y$ , where  $f_0 = -10^{-4} \text{ s}^{-1}$ ,  $\beta = 10^{-11} \text{ s}^{-1} \text{ m}^{-1}$ ,  $L_y = 2000 \text{ km}$ , and  $k_0 = 10^6 \text{ m}^2 \text{ s}^{-1}$ .

Solutions can be found using the method of characteristics – as described in MR – but modified to ensure that the buoyancy mapped down from the surface matches the vertical distribution of the buoyancy on the equatorward flank of the ACC,  $b_N(z)$ . As suggested by the observational study of Karsten and Marshall (2002b), the stratification on the equatorward flank of the ACC is represented by an exponential with an  $e$ -folding depth of  $h_e = 1000 \text{ m}$ , given by

$$b|_{y=L_y} = b_N(z) = b_1 \exp(z/h_e) + b_2 \tag{14}$$

The constants  $b_1$  and  $b_2$  are determined by requiring that  $b_N(z = -h_m) = \Delta b$  and  $b_N(z = -h) = 0$ , where  $h$  is the depth of the model thermocline at  $y = y_L$ .

An algebraic transformation shows that the isopycnals in Eq. (10) can be represented by the characteristics of a partial differential equation, with characteristic velocities  $v_c$  and  $w_c$  given by

$$\begin{cases} \frac{dy}{dt} = v_c = 1, \\ \frac{dz}{dt} = w_c = s_\rho = -\sqrt{-\frac{\tau_0}{fk_0} - \frac{\psi_{\text{res}}}{k_0}}. \end{cases} \quad (15)$$

Moreover, by Eq. (4),  $\psi_{\text{res}}$  and  $\bar{b}$  do not change at a point moving along the characteristics.

Integration of Eq. (15) requires knowledge of both buoyancy and the residual streamfunction at the bottom of the mixed layer ( $z = -h_m$ ). This suggests the following iterative procedure. First we make an initial guess for  $\psi_{\text{res}}(y)$  (in the following calculation we start with  $\psi_{\text{res}} = 0$ ), compute the characteristics given by (15), and then compare the resulting vertical buoyancy distribution at  $y = L_y$  with our target buoyancy distribution Eq. (14). Then, noting that an increase (decrease) in  $\psi_{\text{res}}$  tends to flatten (steepen) the isotherms, we reduce the error in  $b_N(z)$  by adjusting our initial guess for  $\psi_{\text{res}}(z = -h_m)$ . Integration along characteristics, followed by adjustment of  $\psi_{\text{res}}$ , is then repeated consecutively until the model converges, within the round-off error, to a sought-after solution.

Fig. 8 shows the resulting distribution of buoyancy and residual circulation. Note how  $b_N(z)$  has an exponential form, as required. We see that an overturning circulation of some 18 Sv is found, and in the sense expected from consideration of Fig. 7. The meridional thickening and thinning of isopycnal surfaces in this solution is just as intuited in Fig. 7.

#### 4.2. Solving for the surface buoyancy distribution

Rather than prescribing  $b_m(y)$  at the surface, a more physically realistic model is to solve for it whilst prescribing buoyancy at the Northern flank  $b_N(z)$ . We assume  $b_m$  is set by the interaction with the atmosphere given by Eq. (5), but with the buoyancy flux parameterized thus

$$\tilde{B}_0 = -\lambda(b_m - b^*); \quad b^* = (y/L_y)\Delta b, \quad \Delta b = 0.015 \text{ m s}^{-2}. \quad (16)$$

In the following calculation we use  $\lambda = 3 \times 10^{-6} \text{ s}^{-1}$ , which, if  $h_m \sim 100 \text{ m}$ , corresponds to a relaxation time-scale of several months: the resulting solutions show very little sensitivity to the specific value of  $\lambda$ . The problem

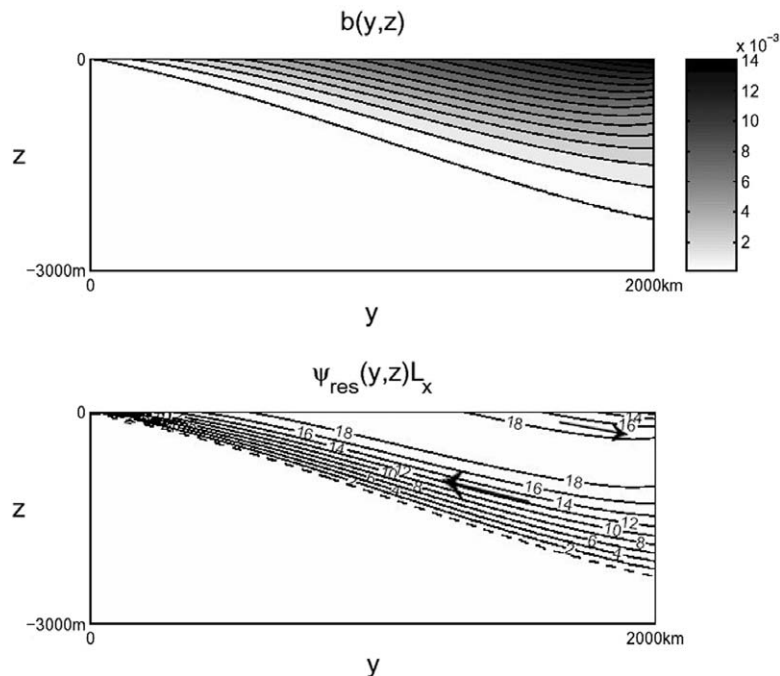


Fig. 8. The buoyancy  $b$  and residual circulation  $\Psi_{\text{res}}$  (in Sv) for a model with a prescribed buoyancy distribution at the surface (linear) and at the Northern flank (exponential).

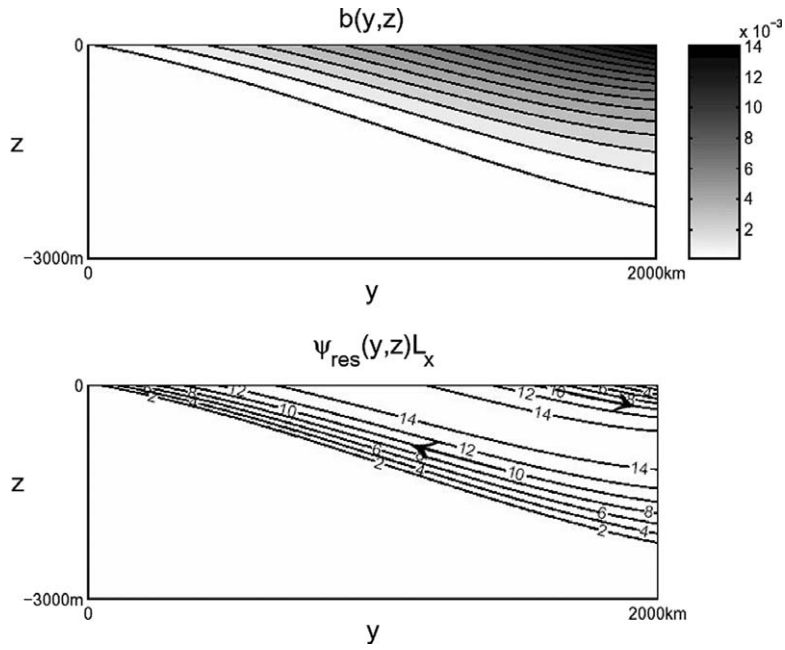


Fig. 9. Buoyancy (top) and  $\psi_{\text{res}}$  (bottom), as in Fig. 8, but for case when the surface buoyancy is relaxed to a linear  $b^*$ , as in Eq. (16), rather than prescribed.

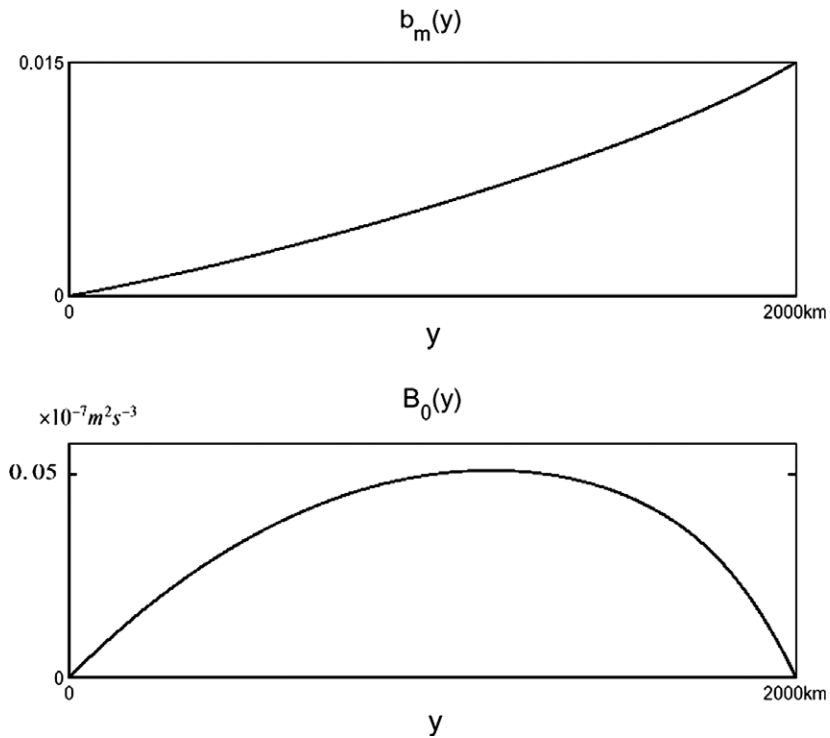


Fig. 10. Surface buoyancy and the surface buoyancy flux for the solution shown in Fig. 9. These fields are not prescribed but obtained as part of the solution. They capture the broad features seen in the observations shown in Fig. 3.

is again solved iteratively; on each iteration the surface buoyancy is readjusted to reduce the error in the computed vertical buoyancy distribution on the Northern flank of the ACC.

The resulting distribution of buoyancy and residual circulation is shown in Fig. 9 and is very similar to the foregoing solutions. The implied air-sea buoyancy flux and the surface buoyancy is shown in Fig. 10. There is an air-sea buoyancy flux directed in to the ocean along the ACC with a maximum amplitude of  $5 \times 10^{-9} \text{ m}^2 \text{ s}^{-3}$ , broadly in accord with Fig. 3(bottom).

Finally, to make a further contact point with observations, Fig. 11, plots  $\psi_{Ek}$ ,  $\psi_{res}$  and  $\psi^*$  from the solution shown in Fig. 9, along with estimates of the same quantities deduced from observations of surface winds and surface buoyancy fluxes, averaged along observed time-mean geostrophic contours over the southern ocean – details of the observational estimates are given in Marshall et al. (in press). This figure acts as a useful summary of the dynamical balances at work in the southern ocean. The action of the surface westerly wind driving fluid away from Antarctica in the surface Ekman layer, is in large part compensated by eddy-induced

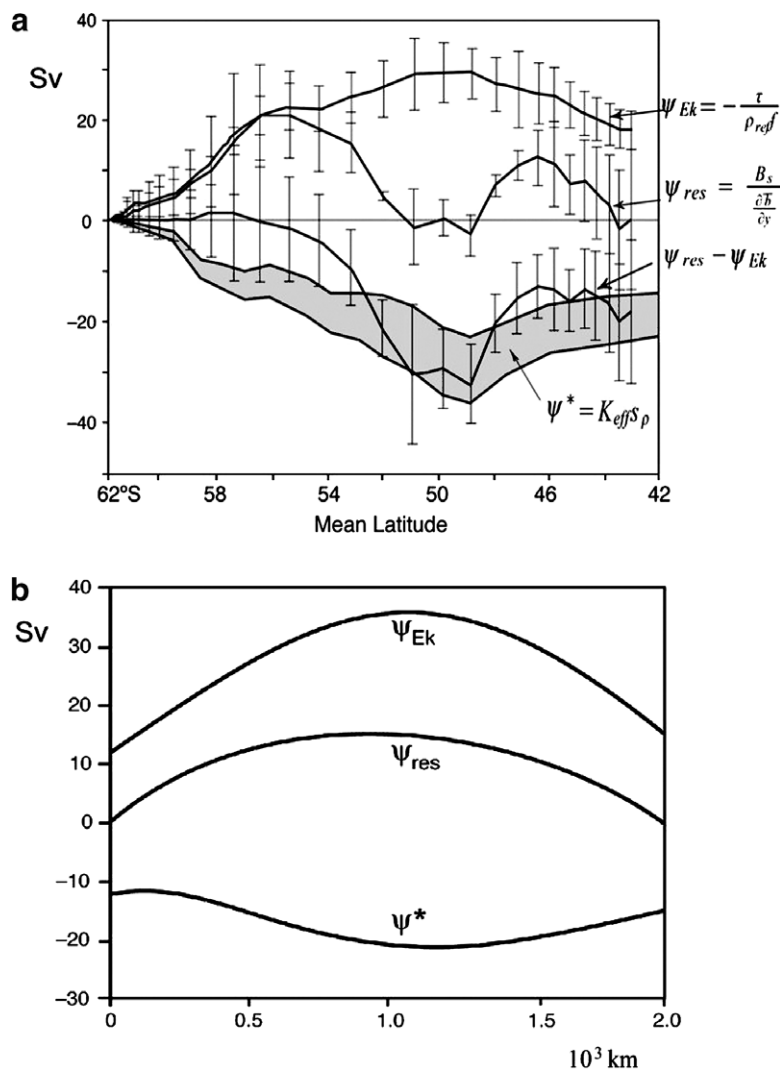


Fig. 11. (a) Estimates of  $\psi_{Ek}$ ,  $\psi_{res}$ ,  $\psi_{res} - \psi_{Ek}$  and  $\psi^*$  deduced from observations of winds and air-sea buoyancy fluxes in the southern ocean. All quantities are averaged around the globe along time-mean streamlines given by altimetry. Estimates of  $\psi^*$  lie in the grey shaded area and depend, as described in Marshall et al. (in press), on the value assumed for the surface eddy diffusivity. The mean position of the axis of the Antarctic Circumpolar Current is at 53° S. (b) Plots of  $\psi_{Ek}$ ,  $\psi_{res}$  and  $\psi^*$  from the solution plotted in Fig. 8.

circulation acting in the opposite direction, leading to a considerably weaker residual flow with upwelling on the poleward flank of the current and downwelling equatorward of the axis of the ACC.

*4.2.1. Sensitivity of solutions to parameter choices*

Perhaps the most uncertain parameter in our simple model is  $k_0$  in Eq. (15), which controls the magnitude of the eddy transfer coefficient, as defined in Eq. (8). Thus in Fig. 12a we plot the maximum value of  $\psi_{\text{resmax}}$ , a measure of the vigor of the overturning circulation, against  $k_0$ , and the associated  $K$ . A value of  $k_0 = 10^6 \text{ m}^2 \text{ s}^{-1}$  was used in the reference solution, yielding a  $K_{\text{max}}$  of  $\sim 10^3 \text{ m}^2 \text{ s}^{-1}$ . As  $k_0$  is increased,  $\psi_{\text{resmax}}$  decreases and  $K$  increases. Values of  $K_{\text{max}}$  that exceed  $2 \rightarrow 3 \times 10^3 \text{ m}^2 \text{ s}^{-1}$  are probably not tenable – see recent estimates of eddy diffusivity inferred by tracer dispersion in the ACC by Marshall et al. (in press) – suggesting that  $\psi_{\text{resmax}}$  is likely to have a strength of  $10 \rightarrow 15 \text{ Sv}$ . Fig. 12b plots the sensitivity of  $\psi_{\text{resmax}}$  to the  $e$ -folding depth,  $h_e$ , of the prescribed stratification on the northern branch of the ACC, keeping  $k_0$  fixed at  $10^6 \text{ m}^2 \text{ s}^{-1}$ . We see that as  $h_e$  increases,  $\psi_{\text{resmax}}$  decreases. Observations in Karsten and Marshall (2002b), suggests that  $h_e = 1000 \text{ m}$  on the equatorward flank of the ACC – see Fig. 6(bottom). A 20% change (due to, say, a persistent change in the wind stress in the subtropics of the southern ocean) changes the overturning by an amount  $\pm 3 \text{ Sv}$ .

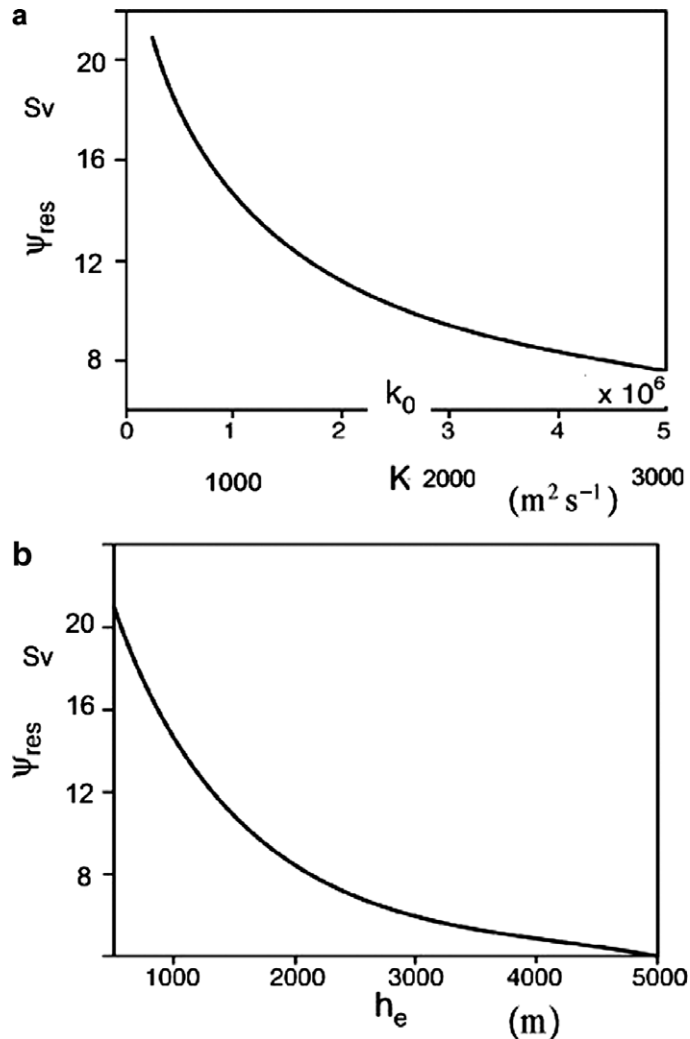


Fig. 12. Sensitivity of  $\psi_{\text{resmax}}$  (in Sv) to (a)  $k_0$  and  $K$  – note different scales (b)  $h_e$ .

## 5. Discussion and conclusions

We have described a simple model of the upper branch of the MOC of the southern ocean in which eddies play a central role in shaping the magnitude and sense of the overturning circulation. We have argued that the action of eddies mixing the large-scale PV gradients set by the geometry of the thermocline ‘wedge’, characteristic of southern-ocean hydrography (see Fig. 2, bottom), inevitably leads to an upper cell as schematized in Fig. 7 and, moreover, demands an air-sea buoyancy flux directed in to the ocean.

The mixed-layer residual buoyancy balance – Eq. (5) – is usually interpreted as a diagnostic relation: given  $B_0$  (and  $b_m$ ), one can infer  $\psi_{\text{res}}$  at the surface of the ocean. Eq. (5) does indeed have great diagnostic value, as shown, for example, by Speer et al.’s (2000) inference of the diabatic Deacon Cell from air-sea fluxes. This is also the spirit of the analytical model of Marshall and Radko (2003) in which a surface buoyancy distribution is mapped down from the surface for a given pattern of wind and air-sea buoyancy flux. In contrast, the present study emphasizes the connection of the southern ocean to the global circulation: poleward-flowing circumpolar deep water on its equatorward flank and the export of Antarctic Intermediate water near the surface. To the extent that this upper branch of the overturning circulation is driven by the action of eddies on interior IPV gradients, the sense of the air-sea buoyancy flux could be considered to be a consequence of internal ocean dynamics, rather than being imposed on it from the meteorology above. Could the band of air-sea buoyancy flux directed in to the ocean along the axis of the ACC, so evident in observations (see, e.g. Fig. 3 bottom), be a consequence of underlying ocean dynamics? This is perhaps best discussed in the context of simple coupled models, an investigation of which is underway.

Finally, the simple model presented here suggests that if  $b_N(z)$  – the stratification on the equatorial flank of the ACC – is sensitive to the pattern of Ekman pumping on the equatorial flank, as might be expected if LPS dynamics pertains in the gyre regime, then the wind field outside the region of circumpolar flow could play an important role in modulating the strength of the meridional overturning circulation *within* the circumpolar region. This may have myriad implications for understanding how the overturning circulation of the southern ocean might have been different in other climates and how variability in the southern ocean’s MOC might be driven.

## Acknowledgements

This work was supported by the Polar Programs Division of the National Science Foundation. We thank two helpful reviewers for their comments.

## Appendix

The discussion in Section 3.1 centered around constant potential vorticity solutions on the  $f$ -plane. But what happens if we suppose that on the  $\beta$ -plane eddies mix potential vorticity rather than thickness? If PV is uniform then

$$\frac{ds_\rho}{dz} = \frac{\beta}{f}$$

where  $\beta = \frac{df}{dy}$ . Integrating in  $z$  and applying boundary conditions at the base of the mixed layer we find

$$s_\rho = \frac{dz}{dy} = s_{\rho-h_m}(y) + \frac{\beta}{f}z.$$

instead of Eq. (11). Noting that isopycnals have zero depth at  $y = 0$ , the above has solution

$$z = \frac{f}{\beta} s_{\rho-h_m}(y) \left( e^{\frac{\beta L y}{f}} - 1 \right) \quad (17)$$

Fig. 13 plots  $\frac{f}{\beta} \left( e^{\frac{\beta L y}{f}} - 1 \right)$  for three values of  $\frac{\beta L}{f}$ . Typically  $\frac{\beta L}{f} \approx 0.2$  in the southern ocean and so we conclude that in the limit  $\frac{\beta L}{f} \ll 1$ , the constant PV solution on the  $\beta$ -plane is very similar to the constant PV solution on the  $f$ -plane: Eq. (17) essentially reduces to Eq. (5).

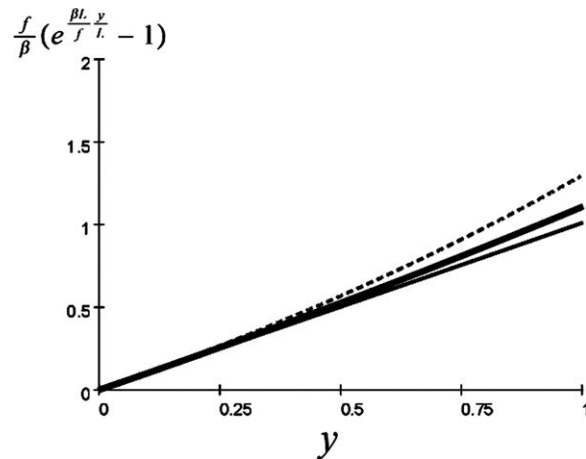


Fig. 13. Plot of  $\frac{f}{\beta} \left( e^{\frac{\beta y}{l}} - 1 \right)$  for  $\frac{\beta l}{f} = 0.02$  (thin),  $\frac{\beta l}{f} = 0.2$  (thick), and  $\frac{\beta l}{f} = 0.5$  (dotted).

## References

- Andrews, D., McIntyre, M., 1976. Planetary waves in horizontal and vertical shear: the generalized Eliassen–Palm relation and the zonal-mean acceleration. *J. Atmos. Sci.* 33, 2031–2048.
- Andrews, D.G., Holton, J., Leovy, C., 1987. *Middle Atmosphere Dynamics*. Academic Press, 489pp.
- Cenedese, C., Marshall, J., Whitehead, J.A., 2004. A laboratory model of thermocline depth and exchange across circumpolar fronts. *J. Phys. Oceanogr.* 34 (3), 656–667.
- Cessi, P., Fantini, M., 2004. The eddy-driven thermocline. *J. Phys. Oceanogr.* 34 (12), 2642–2658.
- Gnanadesikan, S., 1999. A simple predictive model for the structure of the oceanic pycnocline. *Science* 283, 2077–2079.
- Johnson, G.C., Bryden, H.L., 1989. On the size of the Antarctic Circumpolar Current. *Deep Sea Res.* 36, 39–53.
- Karsten, R., Marshall, J., 2002a. Inferring the residual circulation of the Antarctic circulation current from observations using dynamical theory. *J. Phys. Oceanogr.* 32 (12), 3315–3327.
- Karsten, R., Marshall, J., 2002b. Testing theories of the vertical stratification of the ACC against observations. *Dyn. Atmos. Ocean.* 36, 233–246.
- Luyten, J., Pedlosky, J., Stommel, H., 1983. The ventilated thermocline. *J. Phys. Oceanogr.* 13, 292–309.
- Marshall, D., 1997. Subduction of water masses in an eddying ocean. *J. Mar. Res.* 55, 201–222.
- Marshall, J., Radko, T., 2003. Residual mean solutions for the Antarctic Circumpolar Current and its associated overturning circulation. *J. Phys. Oceanogr.* 33 (11), 2341–2354.
- Marshall, J., Jones, H., Karsten, R., Wardle, R., 2002. Can eddies set ocean stratification? *J. Phys. Oceanogr.* 32 (1), 26–38.
- Marshall, J., Shuckburgh, E., Jones, H., Hill, C., in press. Estimates and implications of near-surface eddy diffusivities deduced by tracer transport in the southern ocean. *J. Phys. Oceanogr.* 36 (9).
- McDougall, T.J., McIntosh, P.C., 1996. The temporal-residual-mean velocity. Part I: Derivation and the scalar conservation equations. *J. Phys. Oceanogr.* 26 (12), 2653–2665.
- McDougall, T.J., McIntosh, P.C., 2001. The temporal-residual-mean velocity. Part II: Isopycnal interpretation and the tracer and momentum equations. *J. Phys. Oceanogr.* 31 (5), 1222–1246.
- Olbers, D., Visbeck, M., 2005. A model of the zonally-averaged stratification and overturning in the southern ocean. *J. Phys. Oceanogr.* 35 (7), 1190–1205.
- Rhines, P.B., Young, W.R., 1982. Homogenization of potential vorticity in planetary gyres. *J. Fluid Mech.* 122 (SEP), 347–367.
- Rintoul, S., Hughes, C., Olbers, D., 2001. The Antarctic Circumpolar Current system (Chapter 4.6). In: *Ocean Circulation and Climate*. In: Siedler (Ed.), *International Geophysics Series*, vol. 77. Church and Gould.
- Sloyan, B.M., Rintoul, S.R., 2001. The Southern Ocean limb of the global deep overturning circulation. *J. Phys. Oceanogr.* 31 (1), 143–173.
- Speer, K., Rintoul, S.R., Sloyan, B., 2000. The diabatic Deacon Cell. *J. Phys. Oceanogr.* 30 (12), 3212–3222.
- Sverdrup, H.U., Johnson, M.W., Fleming, R.H., 1942. *The Oceans, Their Physics, Chemistry, and General Biology*. Prentice Hall, 1087pp.
- Toggweiler, J.R., Samuels, B., 1998. On the ocean's large-scale circulation near the limit of no vertical mixing. *J. Phys. Oceanogr.* 28 (9), 1832–1852.
- Visbeck, M., Marshall, J., Haine, T., Spall, M., 1997. Specification of eddy transfer coefficients in coarse-resolution ocean circulation models. *J. Phys. Oceanogr.* 27 (3), 381–402.